HHS Public Access

Author manuscript

Neuron. Author manuscript; available in PMC 2016 June 07.

Published in final edited form as:

Neuron. 2011 July 14; 71(1): 49–60. doi:10.1016/j.neuron.2011.05.030.

The functional neuroanatomy of object agnosia: A case study

Christina S. Konen[1], **Marlene Behrmann**[2], **Mayu Nishimura**[2], and **Sabine Kastner**[1]

[1]Department of Psychology and Princeton Neuroscience Institute, Princeton University, Princeton, NJ 08540, USA

[2]Department of Psychology, Carnegie Mellon University, Pittsburgh, PA 15213, USA

Summary

Cortical re-organization of visual and object representations following neural injury was examined using fMRI and behavioral investigations. We probed the visual responsivity of the ventral visual cortex of an agnosic patient who was impaired at object recognition following a lesion to the right lateral fusiform gyrus. In both hemispheres, retinotopic mapping revealed typical topographic organization and visual activation of early visual cortex. However, visual responses, object-related and -selective responses were reduced in regions immediately surrounding the lesion in the right hemisphere, and also, surprisingly, in corresponding locations in the structurally intact left hemisphere. In contrast, hV4 of the right hemisphere showed expanded response properties. These findings indicate that the right lateral fusiform gyrus is critically involved in object recognition and that an impairment to this region has widespread consequences for remote parts of cortex. Finally, functional neural plasticity is possible even when a cortical lesion is sustained in adulthood.

Introduction

Converging evidence from neuroimaging studies indicates that the ventral visual pathway is important for object recognition (Grill-Spector et al., 1999; Malach et al., 1995). Intermediate hV4 evinces responses that are object-selective but viewpoint- and size-specific, suggesting that the underlying neural populations are tuned to lower-level features of an object (Grill-Spector et al., 1999; Konen and Kastner, 2008), whereas higher-order LOC responds selectively to objects independent of image transformations, suggesting a more abstract visual representation that is necessary for perceptual object constancy (James et al., 2002; Konen and Kastner, 2008). Further support for the integral role of this pathway in object recognition is gleaned from studies showing that the extent of BOLD activation in these areas and object recognition are correlated (James et al., 2000; Bar et al. 2001). However, the neuroimaging findings do not establish a causal relationship between these regions and behavior. The more compelling causal evidence stems from electrical stimulation and patient studies. These studies have shown that electrical stimulation of LOC in epileptic patients, implanted with electrodes for seizure focus localization, interferes with object recognition (Puce et al., 1999) and that lesions of these regions produce deficits in object recognition (Damasio et al., 1990).

Address for Correspondence: Christina S. Konen, Department of Psychology, Princeton University, Princeton, NJ 08540, USA, ; Email: ckonen@princeton.edu

A deficit in object recognition despite intact intelligence is termed object agnosia. Importantly, object agnosia is not attributable to a general loss of knowledge about the object, as auditory and tactile recognition of the very same objects are preserved. Object agnosia may be accompanied by impaired face recognition (prosopagnosia), although this varies considerably across individuals (Farah, 1994). An ongoing, controversial issue concerns the neuroanatomical basis of object agnosia, with open issues concerning the site of the lesion. For example, some studies have documented agnosia after a lesion of the right hemisphere (RH; Humphreys and Riddoch, 1984) whereas others have reported agnosia after left hemisphere (LH) damage (De Renzi, 2000). The majority of case studies, however, report agnosia following bilateral lesions of ventrolateral or ventromedial occipito-temporal cortex (Goodale et al., 1991; McIntosh et al., 2004; Karnath et al., 2009). Also, because the lesion/s are large in most cases, demarcating the critical lesion site for agnosia remains elusive. Understanding the neuroanatomical basis of object agnosia promises to elucidate the neural correlates of object agnosia and to shed light on the mechanisms critically subserving normal object recognition.

We performed a comprehensive case study of patient SM, who, following an accident that resulted in selective brain damage, suffers from profound object agnosia and prosopagnosia with preserved lower-level vision. To explore alterations in the responsiveness of the cortical tissue in and around the lesion site and in anatomically corresponding regions of the intact hemisphere, we documented the organization of SM's retinotopic cortex and analyzed the lesion site relative to the bounds of early visual areas. We then determined the functional consequences of the lesion on cortical tissue as a function of proximity to the lesion site and as a function of topographic location by contrasting cortical responses to visual stimuli relative to blank images and intact objects relative to scrambled objects. Finally, we analyzed the object selectivity of object-responsive cortical regions using an fMRI adaptation (fMR-A) paradigm. This fine-grained approach enabled us to compare the lesioned region with mirror-symmetric locations in SM's non-lesioned hemisphere, and to compare the lesion and surrounding cortex with anatomically equivalent locations in control subjects. To our knowledge, this study constitutes the most extensive functional analysis of the neural substrate underlying object agnosia and offers powerful evidence concerning the neural representations mediating object perception in normal vision.

Results

Functional topography of retinotopic cortex

To define the lesion site relative to retinotopic cortex in SM, we performed phase-encoded retinotopic mapping using standard procedures (see Experimental Procedures). Fig. 1 shows the polar angle representations overlaid on flattened surface reconstructions in SM and a single control subject (C1). In early visual cortex, 6 distinct topographically organized cortical areas were defined in SM (Fig. 1A). These areas have been reported in healthy subjects (Sereno et al., 1995) and can also be seen in C1 (Fig. 1B).

The projection of the lesion onto the reconstructed surface of SM's posterior cortex revealed that it was located anterior to hV4 and dorsolateral to VO1/2 (Fig. 1A). Anatomically, the lesion site was confined to a circumscribed region in the posterior part of the lateral fusiform

gyrus in the RH and comprised a volume of 990 mm^3 (Talairach-coordinates: +44, -46, -2). Functionally, the lesion was located within LOC, which is typically defined by contrasting object versus scrambled image presentations (Malach et al., 1995).

Activation patterns in visual cortex

First, we investigated activation patterns evoked by visual stimuli compared to a blank image (visually-responsive activations) and by object stimuli compared to scrambled objects (object-responsive activations). Different types of object stimuli were used including 2D- and 3D-objects, line drawings of objects, 2D-objects in different sizes and 3D-objects in different viewpoints (Fig. 2). 2D-objects were used to assess cortical responsivity for geometric objects, 3D-objects were used to test complex objects and line drawings of objects were used to probe semantically meaningful stimuli. To dissociate high- from low-level object representations, invariant properties for the size of 2D-objects and the viewpoint of 3D-objects were investigated.

Regions-of-interest (ROIs) within early retinotopic cortex, including V1, V2, V3, V3A, hV4, and VO1/2 were defined by their topographic organization, whereas ROIs beyond early retinotopic cortex were classified by their anatomical location. Fig. 3A shows visually-responsive activation maps ($P<0.001$) of the flattened RH in SM and C1. C1 exhibited activation in hV4 and LOC that was representative of the group and allowed single-subject comparisons with SM. Activation maps of flattened surfaces of both hemispheres are shown for SM and 3 control subjects (C1-C3) in Supplementary Fig. 1. Fig. 4 shows anatomical views of SM's lesion site in sagittal (Fig. 4A) and axial planes without (Fig. 4B) and with (Fig. 4C) marking of the lesion. Visually-responsive activation maps in anatomical space ($P<0.001$) are shown in Fig. 4D. Activated volumes, defined by the number of significantly activated voxels in a given ROI, are shown in Supplementary Table 1 for the control group, SM, and C1. There were no significant differences between SM and the control group nor between SM and C1 in the extent of the activated volumes within or beyond early retinotopic cortex ($P>0.05$). This finding was confirmed by comparing the activated volumes in SM with a larger group of control subjects (Supplementary Fig. 2), indicating that SM's visual responses in early retinotopic cortex of both hemispheres fell within the distribution of normal subjects.

Next, we investigated object-responsive cortex (objects versus scrambled objects; $P<0.001$). Fig. 3B shows the activation maps of the flattened RH in SM and C1 (see Supplementary Fig. 3 for flattened surfaces of both hemispheres for SM and C1-C3; for anatomical views of SM's occipito-temporal cortex, see Fig. 4E). The extent of the activated volumes for the group, SM, and C1 within and beyond early retinotopic cortex are given in Supplementary Table 1. Comparing activated volumes within early retinotopic cortex revealed no differences between SM and the control group nor between SM and C1 ($P>0.05$). Beyond early retinotopic cortex but within occipital cortex, the comparison of activated volumes revealed no differences between SM and the group, nor between SM and C1 ($P>0.05$). In contrast, activated volumes in temporal and parietal cortex of SM were significantly reduced compared to the group and to C1, respectively ($P<0.05$).

Taken together, SM's overall responsiveness to visual stimulation was not differentiable from that of the controls. In contrast, object-related activity, in temporal and parietal cortex but not occipital cortex, was significantly weaker in SM than in control subjects.

Functional organization of cortex surrounding the lesion

The analysis thus far focusing on the activated volumes provided a large-scale assessment of the functional response characteristics of SM. Next, we performed a similar analysis focusing on cortical tissue surrounding SM's lesion that was not defined by retinotopic organization. To assess this cortical tissue systematically, we defined a rectangular grid that was placed relative to the lesion and consisted of 60 sectors located in 6 columns along the anterior-posterior dimension and 10 rows along the dorsal-ventral dimension. Each sector was 216 mm^3 containing a maximum of 8 voxels and was subsequently used as an ROI for further analyses (Fig. 5A). In SM's RH, the lesion was covered by the 4 central sectors of the 2 posterior columns. Anatomically equivalent locations in control subjects were also probed. Accordingly, the 4 sectors covering the lesion in SM's RH were centered on the posterior tip of the right lateral fusiform gyrus in each subject. Fig. 5B shows the position of the grid in control subject C1. Posterior and ventral sectors of the grid covered parts of VO1/2, while dorsal sectors covered most parts of functionally localized LOC, which was defined on the basis of anatomical and functional characteristics. As in previous studies (e.g., Malach, et al. 1995), LOC was defined as a contiguous cluster localized near the lateral occipital sulcus that responded more strongly to the presentations of intact pictures of objects versus their scrambled counterparts ($P<0.0001$). LOC was separately defined for each fMRI-study. For example, 2D-objects were contrasted with scrambled 2D-objects (Fig. 2A-B). For the functional analysis of grid-sectors, the 4 sectors encompassing the lesion site were excluded. It is important to note that the grid analysis does not assume or require corresponding functional grid locations across subjects, since we probed general response characteristics such as visual responsiveness, object-related and -selective responses, which are typical for this portion of cortex.

Responsiveness to visual stimuli—The visual responsiveness of cortex in the penumbra of the lesion was investigated by contrasting activations evoked by presentations of all types of objects versus blank images (Fig. 5C, Supplementary Table 2). Supplementary Fig. 4 shows the activations evoked by presentations of individual types of objects versus blank images. The criterion for significant activation in a given grid-sector was defined as an activated volume of at least 50% of the grid sector's volume, that is 108 mm^3, or 4 voxels ($P<0.001$) for all subsequent analyses. To exclude the possibility that an arbitrary voxel threshold distorted the results, we performed a second analysis with a more lenient voxel threshold of 81 mm^3, or 3 voxels (Supplementary Fig. 5), which yielded similar results compared to the more conservative analysis presented here. In the controls, 79±11% of the grid-sectors in the RH showed activation indicating that cortex covered by the grid responded well to visual stimulation. Similarly, 77% of the grid-sectors in the RH showed visual activation. The sectors that were not visually responsive were located in anterior and ventral sectors of the grid. Eccentricity maps from the control subjects suggested that these locations represent the periphery as opposed to the fovea of the visual field (Arcaro et al., 2009). Thus, the lack of activation in these regions is likely due to the parafoveal location of

the stimuli. In SM, 64% of the sectors in the RH showed activation. Interestingly, most sectors immediately surrounding the lesion were activated and sectors that were not responsive to visual stimulation, as in the control subjects, were located in anterior and ventral sectors of the grid. A comparison of the number of activated sectors during presentations of all types of objects as well as during presentations of individual types of objects between the group and SM, as well as SM and C1, revealed no significant differences ($P>0.05$; Supplementary Table 2).

Responsiveness to object stimuli—Object-responsive activations within the grid were investigated by contrasting intact objects with their scrambled counterparts (Fig. 5D, Supplementary Table 2). In the control group, 66±14%, and similarly in C1, 70% of the sectors in the RH showed object-related responses. Most of the sectors that were not responsive to the presentation of object stimuli were located in anterior and ventral sectors of the grid, thus in cortical regions that likely represent the periphery of the visual field. In SM, only 11% of the RH sectors showed object-related responses. The number of activated sectors was significantly reduced in SM compared to the control group and to C1 ($P<0.05$), but similar to healthy subjects, sectors that were not responsive were located anterior and ventral to the lesion and thus outside retinotopic cortex and LOC.

Object-selective responses—Object-selective responses were investigated in an fMR-A paradigm. For 2D- and 3D-objects and line drawings, the same object was presented 16 times in the adapted condition, while 16 different objects were presented once in the non-adapted condition. To investigate object-selective responses, we calculated an adaptation index (AI), which estimates the response difference between the adapted and non-adapted conditions. A sample time course of fMRI signals for 2D-objects is shown for SM in Supplementary Fig. 6. Fig. 5E and Supplementary Table 2 show the grid-sectors exhibiting object-selective responses in the control group, SM, and C1. In the group, 68±13% of the grid in the RH showed object-selective responses, and in C1, 61% of the grid in the RH showed object-selective responses, the majority of which were located in posterior and dorsal sectors of the grid and covered LOC. In SM, only 13% of the grid exhibited object-selective responses, which was significantly reduced compared to the control group and to C1 ($P<0.05$). The sectors showing object-selective responses collectively covered LOC and were anatomically located dorsal to the lesion site.

Functional organization of left hemisphere and inter-hemispheric response differences

Patient SM's LH was structurally intact, which allowed us to investigate whether a RH lesion of object-selective cortex may have consequences on anatomically equivalent locations in the contralesional hemisphere. To examine this issue, the 4 sectors of the rectangular grid covering the lesion in SM's RH were centered on the posterior tip of the left lateral fusiform gyrus permitting the comparison of the lesioned RH and mirror-symmetric locations in the structurally intact LH (Fig. 5A). Similar to the analysis of the RH, anatomically equivalent locations in the LH of control subjects were also probed.

Responsiveness to visual stimuli (Fig. 5C, Supplementary Fig. 4)—In the controls, 82±12% of the sectors in the LH showed activation during presentations of objects

versus blank images, confirming that cortex covered by the grid responded well to visual stimulation. In C1, 71% of the grid-sectors in the LH showed visual activation. Similar to the RH, the sectors that were not visually responsive were located in anterior and ventral sectors of the grid, likely due to the parafoveal location of the object stimuli. In SM, 79% of the grid in the LH showed activation, and most of the sectors that were not responsive to visual stimulation were located outside LOC. A comparison of the number of activated sectors during presentations of all types of objects combined as well as during presentations of individual types of objects between the group and SM, as well as SM and C1, revealed no significant differences ($P>0.05$; Supplementary Table 2).

Responsiveness to object stimuli (Fig. 5D)—In the control group, 77±10% of the grid in the LH showed object-related responses. In C1, 70% of the grid in the LH showed object-related responses, which was similar to the group ($P>0.05$). In SM, 30% of the grid in the LH showed object-related responses. Similar to healthy subjects, sectors that were not responsive were located in anterior and ventral sectors of the grid, and thus outside LOC. The number of activated sectors was significantly reduced in SM as compared to the control group and C1 ($P<0.05$). Importantly, a comparison of the number of activated sectors showing object-related responses in the LH and RH revealed no inter-hemispheric differences in the group, SM, or C1 ($P>0.05$).

Object-selective responses (Fig. 5E, Supplementary Table 2)—In the group, 70±12%, and in C1, 61% of the grid showed object-selective responses. Dramatically, in SM, only 4% of the grid in the LH responded in an object-selective manner. Both sectors were located in LOC and hence in posterior and dorsal sectors of the grid. The comparison between the group and SM, and C1 and SM, showed a significant reduction in SM in the number of object-selective sectors ($P<0.01$). The inter-hemispheric comparison of object-selective responses revealed no significant differences between the group, SM, or C1 ($P>0.05$).

It is important to note that the object-selective responses as revealed by the AIs applied to all stimulus types, with reduced object-selective responses in SM compared to the group or to C1 ($P<0.05$). Inter-hemispheric comparisons revealed similar responses in both hemispheres for the group, SM, and C1 ($P>0.05$). Intriguingly, SM showed reduced object-selectivity in the structurally intact LH regions of cortex that were mirror-symmetric to the RH lesion site (2D-objects: 4% vs. 12%; 3D-objects: 6% vs. 18%; line drawings: 4% vs. 10%; 2D-size: 6% vs. 16%; 3D-viewpoint: 2% vs. 8%).

To quantify the inter-hemispheric response profiles, the magnitude of responses to visual stimulation was examined. As a first step, the strength of mean signal changes of each grid-sector was determined. The strength of fMRI responses was significantly reduced for all object stimuli combined as well as for line drawings, 2D-objects in different sizes, and 3D-objects in different viewpoints in SM as compared to the control group and to C1, respectively ($P<0.05$; Fig. 5C, Supplementary Fig. 4), whereas the magnitude of activations was similar for 2D-objects and 3D-objects ($P>0.05$; Supplementary Fig. 4). Together, the results indicated that the strength of fMRI signals in SM was similar to control subjects during presentations of some types of object stimuli, whereas it was reduced during

presentations of others. However, the analysis of AIs revealed reduced adaptation for all types of object stimuli (including 2D- and 3D-objects) indicating that differences in magnitude of visual responses cannot explain differential adaptation effects between SM and control subjects. Next, we correlated the magnitude of visual responses between hemispheres (Fig. 6A) by comparing the mean signal changes of each ROI in the LH with those of the corresponding ROIs in the RH. In SM, the correlation between hemispheres was not significant ($R=0.2$; $P>0.05$). In contrast, in the control group, the correlation between hemispheres was significant ($R=0.6$; $P<0.01$). Correlation coefficients were higher in the control group than in SM ($P<0.05$). Inter-hemispheric differences in SM were also revealed for individual types of object stimuli. The correlation between hemispheres was not significant for line drawings, 2D-objects in different sizes, and 3D-objects in different viewpoints ($R=0.22$, $R=0.37$, and $R=0.21$, respectively; $P>0.05$). In contrast, the correlation between hemispheres was significant for 2D-objects and 3D-objects ($R=0.62$ and $R=0.61$; $P<0.05$). In the control group and C1, inter-hemispheric correlations were significant for all individual types of object stimuli ($P<0.05$).

In order to determine the stage of cortical processing at which the inter-hemispheric differences in SM emerged, we correlated the magnitude of visual responses in retinotopic ROIs (Fig. 6B). For a more detailed analysis, we split early visual areas V1, V2, and V3 into their dorsal and ventral subdivisions. In SM, the mean signal changes of both hemispheres were significantly correlated ($R=0.88$; $P<0.05$). In the control group, the correlation between hemispheres was significant ($R=0.93$; $P<0.05$; Supplementary Fig. 7A). The correlation coefficients between SM and the group were similar ($P>0.05$). In C1, the correlation between both hemispheres was significant ($R=0.89$; $P<0.05$; Supplementary Fig. 7B). The correlation coefficients between SM and C1 were also similar ($P<0.05$). Thus, the inter-hemispheric response differences found in SM appeared to be specific to cortex adjacent to the lesion in the RH and mirror-symmetric locations in the LH, and thus specific to higher-order ventral areas, while lower-order visual areas appeared to respond similarly to those of healthy subjects.

Ventral areas hV4 and LOC

Previously, it has been shown in healthy subjects that both hV4 and LOC exhibit object-selective response properties, with hV4 representing low-level features of an object such as line orientation, while higher-order LOC represents objects independent of image transformations, such as size or viewpoint (Konen and Kastner, 2008). In order to compare the previous study with the present results, response properties at the population level, specifically, in hV4 and LOC, were investigated. In the control group, hV4 showed significant adaptation effects induced by 2D- and 3D-objects as well as by line drawings ($P<0.01$), but not 2D-objects in different sizes or 3D-objects in different viewpoints ($P>0.05$). The AIs of both hemispheres were significantly correlated ($R=0.81$; $P<0.05$; Fig. 7A; Supplementary Table 3). LOC showed adaptation effects evoked by all types of object stimuli including 2D-objects in different sizes and 3D-objects in different viewpoints ($P<0.01$). Again, the hemispheres' responses were significantly correlated ($R=0.64$; $P<0.05$; Fig. 7B; Supplementary Table 3; Supplementary Fig. 8).

In hV4 of SM, however, no significant adaptation effects were found in the LH (P>0.05). In contrast, in the RH, 2D- and 3D-objects as well as 2D-objects in different sizes evoked adaptation effects (P<0.01), whereas line drawings and 3D-objects in different viewpoints induced no adaptation. The AIs were not correlated between both hemispheres (R=0.33; P>0.05; Fig. 7A; Supplementary Table 3). The adaptation profile of LOC was similar to hV4, with no adaptation effects found in the LH (P>0.05). In contrast, in the RH, 2D- and 3D-objects as well as 2D-objects in different sizes evoked adaptation effects (P<0.01), while line drawings and 3D-objects in different viewpoints induced no adaptation. The AIs were not correlated between hemispheres (R=0.5; P>0.05; Fig. 7B; Supplementary Table 3). The correlation coefficients between SM and the group were different (P<0.05).

These results indicated hemispheric asymmetries of intermediate hV4 and higher-order LOC in the ventral pathway of SM. Furthermore, both areas showed similar response profiles. The LH showed no significant adaptation effects, whereas the RH showed adaptation induced by 2D- and 3D-objects as well as 2D-objects in different sizes. Within the RH, adaptation effects induced by 2D- and 3D-objects were similar between SM and the controls. Interestingly, hV4 showed size-invariant response properties in SM, while responses of hV4 in healthy subjects were size-specific. Furthermore, LOC was dependent on the viewpoint of objects in SM, whereas LOC in the controls exhibited viewpoint-invariant response properties. Finally, semantically meaningful line drawings induced no object-selective responses in the ventral pathway of SM.

Correlation between behavior and object-selective responses

To gain insight as to how SM perceived the stimuli that were presented in the fMRI experiments, we tested SM on a Same/Different-Judgment Task and a Naming-Task using the object stimuli from the fMR-A experiments after the scanning experiments were completed. In the Same/Different-Judgment Task, 2 objects were shown for unlimited duration and SM pressed one of two buttons to indicate his response. In separate blocks, the 2 objects were drawn from the set of 2D-objects, 3D-objects, line drawings, 2D-objects in different sizes, and 3D-objects in different viewpoints. SM's latencies for all object types were significantly longer than the controls (P<0.01), but latencies were longest and accuracy lowest for 3D-objects in different viewpoints (Supplementary Table 4). In the Naming Task, nameable 2D-objects and line drawings were presented for unlimited duration. As expected, SM's naming accuracy was significantly poorer than the controls (control subjects 100% with both stimulus types; SM 76% for 2D-objects; 70% for line drawings).

Fig. 8 shows the correlation between the behavioral measurements and the AIs in hV4 and LOC for both hemispheres. Since the small amount of data did not permit formal statistical tests, only a qualitative analysis is offered. This analysis suggests no systematic relationship between SM's performance and residual object selectivity in the LH in neither area (Fig. 8A, C). For example, his recognition of 3D-objects was quite good, while this type of object stimulus induced only weak adaptation. In contrast, SM's behavioral performance and AIs in the RH trended towards a more systematic relationship: the better SM's behavioral performance, the higher the AIs in hV4 and LOC (Fig. 8B, D). His performance on the Same/Different-Task indicated better recognition of 2D- and 3D-objects as well as 2D-

objects in different sizes than of line drawings and 3D-objects in different viewpoints. Similarly, AIs in the RH were higher for 2D- and 3D-objects as well as 2D-objects in different sizes than for line drawings and 3D-objects in different viewpoints. His performance in the Naming-Task indicated a trend for better recognition of 2D-objects than of line drawings. AIs in the RH were greater for 2D-objects than for line drawings. Taken together, this analysis suggests that SM's residual object recognition performance is mediated by areas of the ventral pathway in the RH, a possibility that needs to be substantiated by future studies. Particularly, object selectivity in SM's right hV4 appeared to be consistent with his residual recognition performance. This contrasts with the normal profile, in which object selectivity of LOC accounts for recognition performance, including size- and view-invariance.

Discussion

To shed light on the neural basis of object agnosia, we investigated visual, object-related, and object-selective responses across ventral visual cortex, in a patient with severe object agnosia, following a circumscribed lesion of the right lateral posterior fusiform gyrus. First, there were no differences in the functional organization of retinotopic cortex in SM compared with healthy controls. Second, object-related responses were similar in retinotopic cortex for SM and the controls, but were reduced in SM in temporal and parietal cortex. Third, SM evinced a decrement in object-selective response properties in the cortical tissue in and surrounding the lesion in the RH. Fourth, the RH decrement in object-selective responsivity was also observed in corresponding locations of the structurally intact LH. Finally, SM's residual recognition ability appeared to be consistent with the response properties of right LOC and hV4.

The lesion

We localized SM's structural lesion relative to retinotopically and functionally defined cortical areas. The lesion was situated within LOC, anterior to hV4 and dorsolateral to VO1/2, and was confined to a circumscribed region in the posterior part of the lateral fusiform gyrus in the RH. Typically, this region responds more to intact objects than scrambled objects (Malach et al., 1995) and damage to this circumscribed area is likely the principle etiology of SM's object agnosia.

The precise relationship between lesion localization and agnosia has been difficult to establish to date. For example, although the lesion site of patient DF, a well-known agnosic patient who suffered an hypoxic episode (James et al., 2003), has been well documented in anatomical terms, the lesion was not sited relative to retinotopic cortex. Moreover, DF's lesion is much more distributed than SM's, implicating bilateral damage of ventral occipito-temporal cortex. A similar profile has been reported for agnosic patient JS, whose etiology is one of ischemic stroke; like DF, the extent of the brain damage was extensive and bilateral (Karnath et al., 2009) making it difficult to pinpoint the critical area underlying object recognition.

Our results suggest a resolution to the ongoing controversy regarding whether a unilateral or bilateral lesion is necessary for agnosia (De Renzi, 2000). The current view is that a

unilateral RH lesion may suffice; however, as we show, a structural unilateral RH may suffice for object agnosia but because of the detrimental functional effect on the LH, the outcome essentially mimics a bilateral lesion. This finding raises important issues about whether the focal lesion per se serves as the underpinning of the disorder or whether a reconceptualization in terms of a more distributed neural system might be a better formulation.

The proximal impact of the lesion

The first functional finding concerns the normal retinotopy obtained in SM. Although retinotopic maps can be altered extensively in individuals post-stroke (Dilks et al., 2007), this is not so in SM. Critically, the intact retinotopy in SM precludes the ascription of any altered functionality to a foundational problem such as altered topographical organization.

In addition, SM's visual responses were relatively unperturbed, although object-related responses were reduced in temporal and parietal regions. Consistent with this, there was a reduction in the AIs across the range of object types not only in the region of the lesion, but also in other sectors of the rectangular grid. There is growing recognition that visuoperceptual impairments may arise from lesions to nodes of a distributed ventral occipito-temporal circuit, but also from a disconnection between more posterior and more anterior cortical regions. Although these disconnection studies have focused primarily on prosopagnosia (Thomas et al., 2009), presumably the same connectivity failure can also account for object agnosia (Ffytche et al., 2010). On this account, SM's lesion not only impacts LOC but also the propagation of signal to and from this region.

The distal impact of the lesion

A surprising finding was the profound reduction in object-selectivity in SM's structurally intact LH. As with the RH, the LH evinced normal retinotopic organization, relatively preserved visual responsiveness, but reduced object-related responsiveness. Notably, there was no difference in the number of activated object-related sectors compared to the RH. Although the structurally intact LH had general response properties similar to those found in control subjects, dramatically only 4% of the grid sectors exhibited significant adaptation. In the RH, 13% of the grid sectors exhibited significant adaptation. We interpret this somewhat greater decrement in the LH than RH with caution given that it was based on a single adaptation paradigm.

To our knowledge, there has not been a detailed examination of the contralesional hemisphere in object agnosia. The diminution of object responsivity in the LH might arise for at least two possible reasons. First, given the callosal shearing reported in SM's medical history, there might be no propagation of signal from the damaged RH to the intact LH. This possibility seems implausible for several reasons. First, fMRI signals in early visual cortex were strongly correlated indicating intact propagation of neural signals between the hemispheres and therefore intact callosal connections. Second, there are no structural perturbations in the relevant white matter tracts, as determined by a recent diffusion tensor imaging study of SM, which reported disrupted fiber connections only from the left prefrontal cortex to both the left fusiform gyrus and the right prefrontal cortex (Jung and

Jung, 2010). Importantly, the connections between the posterior regions themselves were intact.

An alternative explanation is that the intact LH was inhibited by the lesioned RH. Inter-hemispheric inhibition is the neurophysiological mechanism by which one hemisphere of the brain inhibits the opposite hemisphere (van Meer et al. 2010). Although plasticity and compensation in some regions of cortex, such as Broca's area, engage the contralateral hemisphere in an excitatory fashion and assist in recovery (Saur et al., 2006), the converse seems to be true in other regions. For example, inter-hemispheric inhibition is well-recognized in motor cortex, and many studies have been devoted to characterizing this phenomenon, even using TMS to reduce the pathological cross-hemispheric inhibition (Williams et al. 2010). Our findings suggest that a similar phenomenon may be at play in SM and, as such, this result opens up a provocative avenue for further research. If this interpretation is correct, the finding that the lack of input from the RH's object-selective cortex led to a breakdown of object-responsive tuning properties in the LH, underlines the dominant role of the RH in object vision. This result is compatible with the growing consensus that a unilateral RH, rather than bilateral, lesion is necessary for object agnosia (Farah, 1994). Our findings suggest, however, that while the RH lesion might be primary, this lesion has remote and widespread consequences, with functional inhibition of homologous regions in the structurally intact hemisphere. Such a pattern raises the question whether the observed brain-behavior correspondence serves as the neural underpinning of the impairment or whether reconceptualizing SM's agnosia in terms of disruption to an interconnected more distributed neural system might be a better characterization of SM's pattern and of agnosia more generally. In keeping with this, recent developments in neuroscience emphasize the fundamental role of widely distributed neural networks for the control of behavior with the recognition that physiological effects of brain injury are dynamic and are best assessed over entire networks rather than just locally at the site of structural damage (Carter et al., 2010).

Reorganization of response properties in hV4?

In normal observers, size- and viewpoint-invariant object representations are observed only at the level of LOC, whereas object-specific lower-level representations are typically found in hV4. This was not the case in SM, as hV4 appeared to be responsive both to lower-level representations but also to some higher-level representations, because it showed size-invariant responses. Interestingly, SM's residual recognition ability seemed to parallel the response properties of both hV4 and LOC in his RH, whereas object recognition in healthy subjects typically parallels the response properties of LOC (Bar et al., 2001). These findings open the possibility that SM's hV4 has been recruited to subserve this more complex set of representations. To our knowledge, this is the first demonstration of a lower-order area assuming the properties of a higher-order area. Although there are many instances of plasticity observed in the visual system, for e.g. changes in V1 in individuals who are congenitally blind (Amedi et al., 2010), there has been rather little research on plasticity in higher-order areas of the cortical visual system (Das and Huxlin, 2010).

In conclusion, detailed functional imaging combined with structural imaging and behavioral studies offer a unique window into the brain-behavior correspondences that subserve object recognition. In particular, we have demonstrated that a region in the posterior part of the lateral fusiform gyrus in the RH is necessary for object recognition, and that damage to this area potentially affects connectivity intrahemispherically to and from this region. The circumscribed lesion also adversely impacts the functional integrity of corresponding regions in the contralesional hemisphere, and there also appears to be some reorganization in the intact regions of the affected hemisphere. These results shed light on the neural substrate mediating object recognition and suggest that the study of agnosia provides a unique window into the neural mechanisms supporting intact recognition.

Experimental Procedures

Subjects

Patient SM (right-handed, male, 36 years old), and 5 control subjects (right-handed, 3 male, 29-36 years old) participated in the fMRI studies, which were performed at the Brain Imaging Research Center (BIRC) Pittsburgh (SM) and Princeton University (control subjects). The control subjects had normal or corrected-to-normal visual acuity and no history of neurological disorder. Each subject participated in 2 scanning sessions to obtain retinotopic maps and to probe object representations in visual cortex. Five additional control subjects (right-handed, male, 29-37 years old) participated in the behavioral experiments, which were performed at Carnegie Mellon University (CMU). All subjects gave informed written consent for participation in the studies, which were approved by the Institutional Review Panels of CMU and Princeton University.

Case history

SM sustained a closed head injury in a motor vehicle accident at the age of 18. CT scans obtained after the accident indicated a contusion in right anterior and posterior temporal cortex accompanied by shearing injury in the corpus callosum and left basal ganglia. SM recovered well after rehabilitation, aside from a persisting visual agnosia and prosopagnosia. SM's object agnosia is evidenced by his object-naming performance in the Boston Naming Test and his mean reaction time per correct item. When he fails to recognize an object, he does not appear to possess any semantic information about this object. His auditory identification of objects is unaffected and he can provide detailed definitions in response to the auditory label of an item that he missed when it was presented visually. SM's prosopagnosia is indicated by his impaired performance in the Benton Facial Recognition Test. SM performs within the normal range on tests of low-level visual processing and shows normal color vision. Further details of his medical and neuropsychological history can be found elsewhere (Behrmann and Kimchi, 2003).

Visual display

The stimuli were generated on a Macintosh OS X computer (Apple Computer; Cupertino, CA) using MATLAB software (The MathWorks; Natick, MA) and Psychophysics Toolbox functions (Brainard, 1997; Pelli, 1997). Stimuli were projected from an LCD projector outside the scanner room onto a translucent screen located at the end of the scanner bore.

Subjects viewed the screen through a mirror attached to the head coil. At the BIRC (SM), the path length between the screen and the mirror was 55 cm. The screen subtended 25° of visual angle both horizontally and vertically. At Princeton University (control subjects), the total path length was 60 cm and the screen subtended 30° horizontally and 26° vertically. A trigger pulse from the scanner synchronized the onset of stimulus presentation to the beginning of the image acquisition.

Visual stimuli and experimental design

Retinotopic mapping—Polar angle representations were measured to delineate visual areas and to evaluate SM's lesion site relative to retinotopically organized cortex. The phase encoding design was similar to procedures widely used for retinotopic mapping (Bandettini et al., 1993; Schneider et al., 2004). A transparent wedge within a dark foreground rotated around a central fixation point. The underlying checkerboard was only visible through the transparent wedge, giving the appearance of a rotating checkerboard wedge (Swisher et al., 2007). The wedge rotated either clockwise or counterclockwise and spanned 1-15° in eccentricity with an arc length of 75°. The chromaticity and luminance of each check of the colored checkerboard alternated at a flicker frequency of 4 Hz. To ensure proper fixation, subjects performed a luminance detection task on the fixation point. Luminance changes of the fixation point occurred every 2 to 5 s for the duration of 0.09 s. SM and control subjects performed with an accuracy of 93% and 91±7%, respectively. Each run was composed of eight 40 s cycles of the rotating wedge. Runs alternated between clockwise and counterclockwise wedge rotation, with a total of 12 runs per scanning session.

Adaptation experiments—Using fMR-A paradigms, we investigated neural representations of different types of objects including 2D-objects, 3D-objects, and line drawings of objects as well as size and viewpoint invariance (Fig. 2). For each fMR-A study, 51 gray-scale images of 2D-objects, 3D-objects, or line drawings were used. The objects were subdivided into a matrix of equally sized rectangulars (25 along the horizontal dimension and 25 along the vertical dimension). Subsequently, the rectangulars were randomly re-arranged resulting in 51 scrambled images per study. The stimuli subtended approximately 18°×18° of visual angle centered over a fixation point on a gray background. 2D- and 3D-objects were generated with MATLAB software (The MathWorks; Natick, MA); line drawings were chosen from the ClipArt Gallery (http://office.microsoft.com/). For the size-invariance study, the 2D-objects were changed in size, resulting in 16 different sizes of each object over a range of 6.75°×6.75° to 18°×18°. For the viewpoint-invariance study, the 3D-objects were rotated around the y-axis, resulting in 16 different viewpoints of each object covering a range of ±75°. In the adapted condition, the same object was presented 16 times. In the non-adapted condition, 16 different objects were presented once. Similar stimulus sets and fMR-A paradigms have been successfully used in our previous study (Konen and Kastner, 2008).

Each fMR-A study consisted of 3 scans, each of which contained epochs of intact and scrambled object presentations. Each epoch lasted for 16 s and was alternated with equally long blank periods. In each epoch, 16 intact or scrambled objects were presented for 750 ms each interposed with 250 ms blank periods. Each scan started and ended with a blank period

of 16 s. A central fixation point (0.5°) was presented during the whole scanning session. To control for attention effects between adapted and non-adapted conditions, the fixation point changed color briefly (0.15 s) and infrequently (every 3-5 s on average). The subjects' task was to track the number of color changes and to report the number at the end of each scan. Accuracy was 93% for SM and 95±5% for the controls.

Data acquisition and analysis

Using a standard head coil, and identical scanning sequences and protocol parameters, data were acquired with a 3T head scanner (Allegra, Siemens, Erlangen, Germany) at the BIRC and Princeton University. An anatomical scan (MPRAGE sequence; TR=2.5 s; TE=4.3 ms; 1 mm^3 resolution) was acquired in each session to facilitate cortical surface alignments. For the functional studies, functional images were taken with a gradient echo, echoplanar sequence (TR=2 s, TE=30 ms). Thirty-four axial slices (slice thickness=3 mm, gap=0 mm, voxel size=3×3×3 mm^3) were acquired in 12 series of 128 volumes for retinotopic mapping, 3 series of 136 volumes for the 2D-objects experiment, and 104 volumes for the 3D-objects, line drawings, 2D-size, and 3D-viewpoint experiments.

Data were analyzed by using AFNI (http://afni.nimh.nih.gov/afni), FREESURFER (http://surfer.nmr.mgh.harvard.edu), and SUMA (http://afni.nimh.nih.gov/afni/suma). Functional images were motion-corrected to the image acquired closest in time to the anatomical scan (Cox and Jesmanowicz, 1999) and normalized to percentage signal change by dividing the time series by its mean intensity. After normalization, data were projected onto cortical surface reconstructions that were aligned to each of the experimental sessions. Data were spatially smoothed with a 4-mm Gaussian kernel.

For retinotopic mapping, a Fourier analysis was used to identify voxels activated by the task (Bandettini et al., 1993; Schneider et al., 2004). For each voxel, the amplitude and phase, the temporal delay relative to the stimulus onset, of the harmonic at the stimulus frequency was determined by a Fourier transform of the mean time series of the voxel. To correctly match the phase delay of the time series of each voxel to the phase of the wedge stimulus, the response phases were corrected for the hemodynamic lag (3 s). The counterclockwise scans were then reversed to match the clockwise scans and averaged together.

ROIs contained topographic representations of the visual field and were delineated by representations of the vertical and horizontal meridians (Sereno et al., 1995). Early visual areas V1, V2, and V3 were localized in the calcarine sulcus and adjacent cortex. In the dorsal visual pathway, V3A was identified in the transverse occipital sulcus (Tootell et al., 1997). In the ventral visual pathway, topographically organized hV4 and VO1/2 were localized along the collateral sulcus (Brewer et al., 2005; Wade et al., 2002). The retinotopic maps of SM and control subjects were thresholded at $P<0.001$. Note that the flat maps in Fig. 1 were masked regarding the retinotopic organization of these early visual areas.

For the fMR-A studies, square-wave functions matching the time course of the experimental design were convolved with a gamma-variate function and used as regressors of interest in a multiple regression model in the framework of the general linear model. Additional regressors to account for variance due to baseline shifts between time series, linear drifts

within time series, and head motion were included in the regression model. Voxels that responded to visual stimuli were identified by contrasting activations evoked by intact object versus blank image presentations (visually-responsive activations; $P<0.001$). Voxels that responded to object stimuli were identified by activation resulting from the contrast between object versus scrambled image presentations (object-responsive activations; $P<0.001$). Time series of fMRI intensities were averaged over activated voxels within a given ROI and normalized to the mean intensity obtained during blank periods. All time course analyses were performed on unsmoothed data. For each subject, the 6 peak intensities of the fMRI signal obtained during the object presentations were averaged resulting in mean signal changes. Across healthy subjects, the mean signal changes were averaged to yield group data. Statistical significance of percentage signal change was assessed with a one-way repeated measures ANOVA followed by a multiple comparison test on the mean signal changes.

To quantify the adaptation effects, an adaptation index (AI) was computed for each ROI and fMR-A study: $AI=(R_{non\text{-}adapted}-R_{adapted})/(R_{non\text{-}adapted})$; $R_{adapted}$=mean fMRI signal obtained during the adapted condition, $R_{non\text{-}adapted}$=mean fMRI signal obtained during the non-adapted condition. Negative mean signal changes were excluded from index computations. The metric for this AI was chosen, because previous electrophysiological studies in monkeys (De Baene and Vogels, 2010) and fMRI studies in humans (Weiner et al., 2010) have demonstrated that adaptation in inferior temporal cortex behaves similar to a scaling mechanism. Supplementary Fig. 9 shows the adaptation analysis using a ratio measure for the AI $[(R_{non\text{-}adapted}-R_{adapted})/(R_{non\text{-}adapted}+R_{adapted})]$ as used in our previous study (Konen and Kastner, 2008). Both measures for adaptation yielded similar results and revealed reduced object adaptation effects in SM as compared to the control group and control subject C1. Single subject AIs were calculated for each ROI containing voxels that showed significant activation during object versus blank image presentations ($P<0.001$) and then averaged within each ROI to derive group index values. Statistical significance of index values was assessed with a one-sample t-test against zero.

Lesion site

Structural 3D-reconstructions of SM's brain were coded in RGB color space, which allowed us to determine the intensity values of each voxel in occipito-temporal cortex. The intensity values of voxels in healthy tissue ranged between 55 and 82, whereas the intensity values of voxels in lesioned tissue ranged between 41 and 52. On the basis of this criterion, voxels of SM's lesion site were manually marked and defined as an ROI (Fig. 4B, C). This ROI was subsequently projected onto the cortical flat map. His lesion was confined to a circumscribed region in the posterior portion of the lateral fusiform gyrus and comprised a volume of 990 mm^3.

In order to investigate cortex surrounding the lesion site, we created a rectangular grid. The grid consisted of 6 columns along the anterior-posterior dimension and 10 rows along the dorsal-ventral dimension, divided into 60 equally sized sectors. The volume of each sector was 216 mm^3. Together, the rectangular arrangement comprised a volume of 12.960 mm^3 in ventral visual cortex. The grid allowed us to probe responsiveness using an ROI-approach in

SM and in control subjects by placing the grid on anatomically equivalent locations in each hemisphere. Furthermore, by positioning the posterior edge of the grid on the posterior part of the lateral fusiform gyrus, we were able to exclude early visual areas and hV4 from the grid analysis since these areas were separately investigated on the basis of their retinotopic organization.

Statistical comparisons between single case and control group

For statistical comparisons between SM and the control group, the modified independent samples t-test method was used (Crawford and Garthwaite, 2004). This method accounts for the limited size of control groups, as typically used in neuropsychological single-case studies; the individual is treated as a sample of N=1 and, therefore, does not contribute to the estimate of the within-group variance (Crawford and Howell, 1998).

To quantify the relationship between activations of the lesioned RH and the structurally intact LH in SM, Pearson's linear correlation was used. The mean signal changes or AIs of each ROI in the RH were correlated with the values of the corresponding ROI in the LH. For the comparison of correlation coefficients between SM and the control group, inferential statistics for comparisons between the intra-individual measures of association of a patient and a control group were used (Crawford et al., 2003). We applied Fisher's transformation to the coefficients for SM and each subject in the control group assuming that the true values of the transformed correlations followed a normal distribution and differed between subjects. Subsequently, we were able to test the null hypothesis that the true correlation coefficient for the patient was from the same distribution.

Furthermore, we compared SM with a single subject from the control group (C1) whose data were closest to the group average and thus most representative of the group. First, the number of activated voxels in hV4 and LOC during object versus blank image presentations ($P<0.001$) was calculated in each single subject as well as averaged across subjects. Then, the numbers of activated voxels in single subjects were compared to the average of activated voxels across subjects. A t-test for two independent samples was used for statistical comparisons between SM and C1.

Supplementary Material

Refer to Web version on PubMed Central for supplementary material.

References

Amedi A, Raz N, Azulay H, Malach R, Zohary E. Cortical activity during tactile exploration of objects in blind and sighted humans. Restor Neurol Neurosci. 2010; 28:143–156. [PubMed: 20404404]

Arcaro MJ, McMains SA, Singer BD, Kastner S. Retinotopic organization of human ventral visual cortex. J Neurosci. 2009; 29:10638–10652. [PubMed: 19710316]

Bandettini PA, Jesmanowicz A, Wong EC, Hyde JS. Processing strategies for time-course data sets in functional MRI of the human brain. Magn Reson Med. 1993; 30:161–173. [PubMed: 8366797]

Bar M, Tootell RB, Schacter DL, Greve DN, Fischl B, Mendola JD, Rosen BR, Dale AM. Cortical mechanisms specific to explicit visual object recognition. Neuron. 2001; 29:529–535. [PubMed: 11239441]

Behrmann M, Kimchi R. What does visual agnosia tell us about perceptual organization and its relationship to object perception? J Exp Psychol Hum Percept Perform. 2003; 29:19–42. [PubMed: 12669745]

Behrmann M, Marotta J, Gauthier I, Tarr MJ, McKeeff TJ. Behavioral change and its neural correlates in visual agnosia after expertise training. J Cogn Neurosci. 2005; 17:554–568. [PubMed: 15829077]

Brainard DH. The Psychophysics Toolbox. Spat Vis. 1997; 10:433–436. [PubMed: 9176952]

Brewer AA, Liu J, Wade AR, Wandell BA. Visual field maps and stimulus selectivity in human ventral occipital cortex. Nat Neurosci. 2005; 8:1102–1109. [PubMed: 16025108]

Carter AR, Astafiev SV, Lang CE, Connor LT, Rengachary J, Strube MJ, et al. Resting interhemispheric functional magnetic resonance imaging connectivity predicts performance after stroke. Ann Neurol. 2010; 67:365–375. [PubMed: 20373348]

Cox RW, Jesmanowicz A. Real-time 3D image registration for functional MRI. Magn Reson Med. 1999; 42:1014–1018. [PubMed: 10571921]

Crawford JR, Garthwaite PH. Statistical methods for single-case studies in neuropsychology: comparing the slope of a patient's regression line with those of a control sample. Cortex. 2004; 40:533–548. [PubMed: 15259332]

Crawford JR, Garthwaite PH, Howell DC, Venneri A. Intra-individual measures of association in neuropsychology: inferential methods for comparing a single case with a control or normative sample. J Int Neuropsychol Soc. 2003; 9:989–1000. [PubMed: 14738281]

Crawford JR, Howell DC. Regression equations in clinical neuropsychology: an evaluation of statistical methods for comparing predicted and obtained scores. J Clin Exp Neuropsychol. 1998; 20:755–762. [PubMed: 10079050]

Damasio AR, Tranel D, Damasio H. Face agnosia and the neural substrates of memory. Annu Rev Neurosci. 1990; 13:89–109. [PubMed: 2183687]

Das A, Huxlin KR. New approaches to visual rehabilitation for cortical blindness: outcomes and putative mechanisms. Neuroscientist. 2010; 16:374–387. [PubMed: 20103505]

De Baene W, Vogels R. Effects of adaptation on the stimulus selectivity of macaque inferior temporal spiking activity and local field potentials. Cereb Cortex. 2010; 20:2145–2165. [PubMed: 20038542]

De Renzi E. Disorders of visual recognition. Semin Neurol. 2000; 20:479–485. [PubMed: 11149704]

Dilks DD, Serences JT, Rosenau BJ, Yantis S, McCloskey M. Human adult cortical reorganization and consequent visual distortion. J Neurosci. 2007; 27:9585–9594. [PubMed: 17804619]

Farah, M. Visual agnosia. 2nd. Cambridge: MIT Press/Bradford Books; 1994.

Farah, M. Visual agnosia. Cambridge, MA: MIT Press; 2004.

Ffytche DH, Blom JD, Catani M. Disorders of visual perception. J Neurol Neurosurg Psychiatry. 2010; 81:1280–1287. [PubMed: 20972204]

Goodale MA, Milner AD, Jakobson LS, Carey DP. A neurological dissociation between perceiving objects and grasping them. Nature. 1991; 349:154–156. [PubMed: 1986306]

Grill-Spector K, Kushnir T, Edelman S, Avidan G, Itzchak Y, Malach R. Differential processing of objects under various viewing conditions in the human lateral occipital complex. Neuron. 1999; 24:187–203. [PubMed: 10677037]

Humphreys GW, Riddoch MJ. Routes to object constancy: implications from neurological impairments of object constancy. Q J Exp Psychol A. 1984; 36:385–415. [PubMed: 6533691]

James TW, Culham J, Humphrey GK, Milner AD, Goodale MA. Ventral occipital lesions impair object recognition but not object-directed grasping: an fMRI study. Brain. 2003; 126:2463–2475. [PubMed: 14506065]

James TW, Humphrey GK, Gati JS, Menon RS, Goodale MA. The effects of visual object priming on brain activation before and after recognition. Curr Biol. 2000; 10:1017–1024. [PubMed: 10996068]

James TW, Humphrey GK, Gati JS, Menon RS, Goodale MA. Differential effects of viewpoint on object-driven activation in dorsal and ventral streams. Neuron. 2002; 35:793–801. [PubMed: 12194877]

Jung, KJ.; Jung, HS. Organization for Human Brain Mapping. Barcelona, Spain: 2010. A Major Role of The Left Prefrontal Cortex for Face Recognition: Revealed by Disrupted Connections.

Karnath HO, Ruter J, Mandler A, Himmelbach M. The anatomy of object recognition--visual form agnosia caused by medial occipitotemporal stroke. J Neurosci. 2009; 29:5854–5862. [PubMed: 19420252]

Konen CS, Kastner S. Two hierarchically organized neural systems for object information in human visual cortex. Nat Neurosci. 2008; 11:224–231. [PubMed: 18193041]

Malach R, Reppas JB, Benson RR, Kwong KK, Jiang H, Kennedy WA, Ledden PJ, Brady TJ, Rosen BR, Tootell RB. Object-related activity revealed by functional magnetic resonance imaging in human occipital cortex. PNAS USA. 1995; 92:8135–8139. [PubMed: 7667258]

McIntosh RD, Dijkerman HC, Mon-Williams M, Milner AD. Grasping what is graspable: evidence from visual form agnosia. Cortex. 2004; 40:695–702. [PubMed: 15505979]

Pelli DG. The VideoToolbox software for visual psychophysics: transforming numbers into movies. Spat Vis. 1997; 10:437–442. [PubMed: 9176953]

Puce A, Allison T, McCarthy G. Electrophysiological studies of human face perception. III: Effects of top-down processing on face-specific potentials. Cereb Cortex. 1999; 9:445–458. [PubMed: 10450890]

Schneider KA, Richter MC, Kastner S. Retinotopic organization and functional subdivisions of the human lateral geniculate nucleus: a high-resolution functional magnetic resonance imaging study. J Neurosci. 2004; 24:8975–8985. [PubMed: 15483116]

Sereno MI, Dale AM, Reppas JB, Kwong KK, Belliveau JW, Brady TJ, Rosen BR, Tootell RB. Borders of multiple visual areas in humans revealed by functional magnetic resonance imaging. Science. 1995; 268:889–893. [PubMed: 7754376]

Swisher JD, Halko MA, Merabet LB, McMains SA, Somers DC. Visual topography of human intraparietal sulcus. J Neurosci. 2007; 27:5326–5337. [PubMed: 17507555]

Thomas C, Avidan G, Humphreys K, Jung KJ, Gao F, Behrmann M. Reduced structural connectivity in ventral visual cortex in congenital prosopagnosia. Nat Neurosci. 2009; 12:29–31. [PubMed: 19029889]

Tootell RB, Mendola JD, Hadjikhani NK, Ledden PJ, Liu AK, Reppas JB, Sereno MI, Dale AM. Functional analysis of V3A and related areas in human visual cortex. J Neurosci. 1997; 17:7060–7078. [PubMed: 9278542]

van Meer MP, van der Marel K, Wang K, Otte WM, El Bouazati S, Roeling TA, et al. Recovery of sensorimotor function after experimental stroke correlates with restoration of resting-state interhemispheric functional connectivity. J Neurosci. 2010; 30:3964–3972. [PubMed: 20237267]

Wade AR, Brewer AA, Rieger JW, Wandell BA. Functional measurements of human ventral occipital cortex: retinotopy and colour. Philos Trans R Soc Lond B Biol Sci. 2002; 357:963–973. [PubMed: 12217168]

Weiner KS, Sayres R, Vinberg J, Grill-Spector K. fMRI-adaptation and category selectivity in human ventral temporal cortex: regional differences across time scales. J Neurophysiol. 2010; 103:3349–3365. [PubMed: 20375251]

Williams JA, Pascual-Leone A, Fregni F. Inter-hemispheric modulation induced by cortical stimulation and motor training. Phys Ther. 2010; 90:398–410. [PubMed: 20110339]

Highlights

- Unilateral lesion of lateral fusiform gyrus in right hemisphere causes object agnosia;
- Agnosic patient exhibits normal retinotopy and visual responsivity in visual cortex;
- Object-responsive and object-selective responses are reduced in both hemispheres;
- Cortical plasticity evident with reorganization of intermediate & higher-order areas.

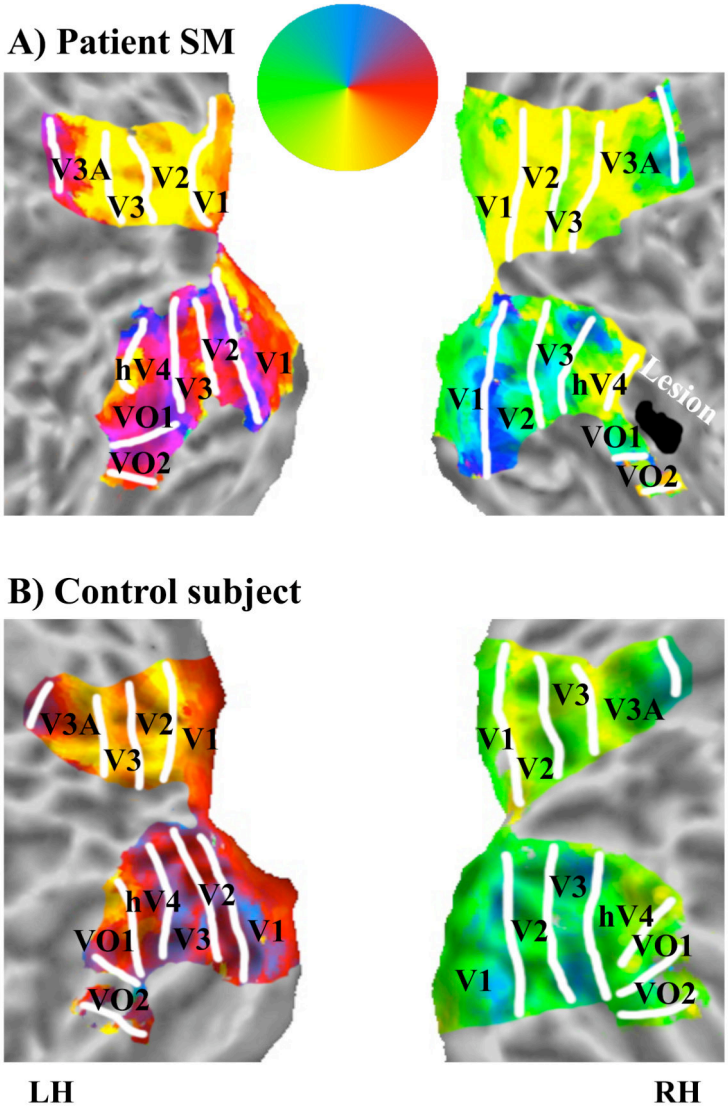

Figure 1. Topographically organized areas and lesion site in SM (A) and control subject C1 (B)

Flattened surface reconstructions of early and ventral visual cortex. The color code indicates the phase of the fMRI response and region of visual field to which underlying neurons responded best. Retinotopic mapping revealed regular patterns of phase reversals in both hemispheres of SM that were similar to healthy subjects such as C1. SM's lesion is shown in black, located anterior to hV4 and dorsolateral to VO1/2. LH=left hemisphere; RH=right hemisphere.

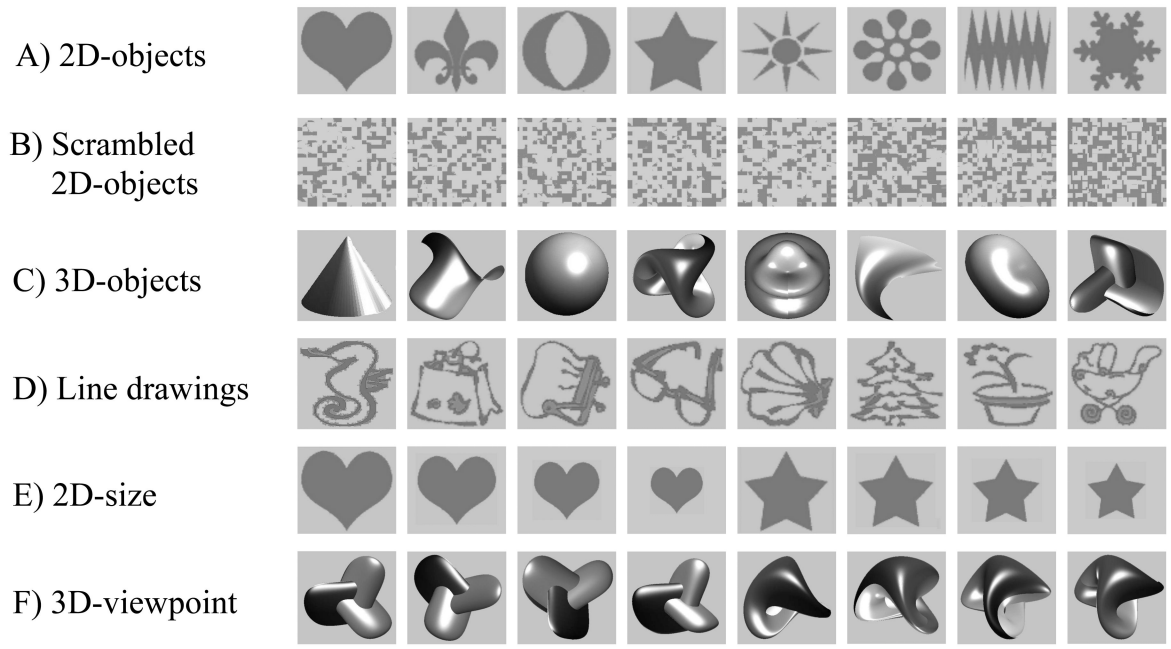

Figure 2. Examples of object stimuli

(A) 2D-objects. (B) Scrambled 2D-objects, as derived from objects in A. (C) 3D-objects. (D) Line drawings of objects. (E) 2D-size. (F) 3D-viewpoint.

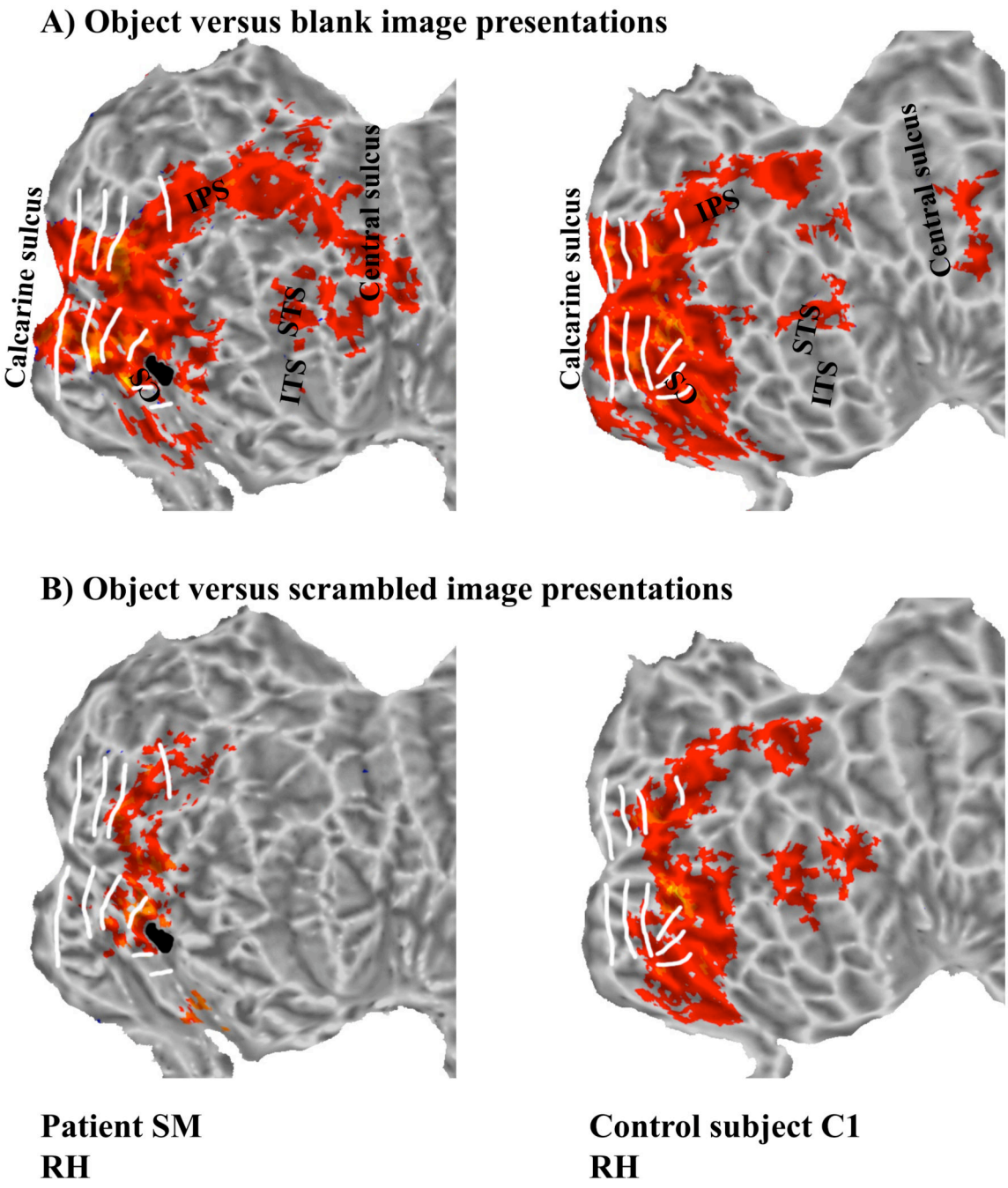

Figure 3. Activations in the right hemispheres of SM (left) and control subject C1 (right). (A) Visually-responsive activations

In SM, activated volumes were similar to those of control subjects. *(B) Object-responsive activations.* In SM, activated volumes in retinotopic cortex were similar to those of control subjects, but reduced in temporal and parietal. CS=collateral sulcus; IPS=intraparietal sulcus; ITS=inferior temporal sulcus; STS=superior temporal sulcus; RH=right hemisphere.

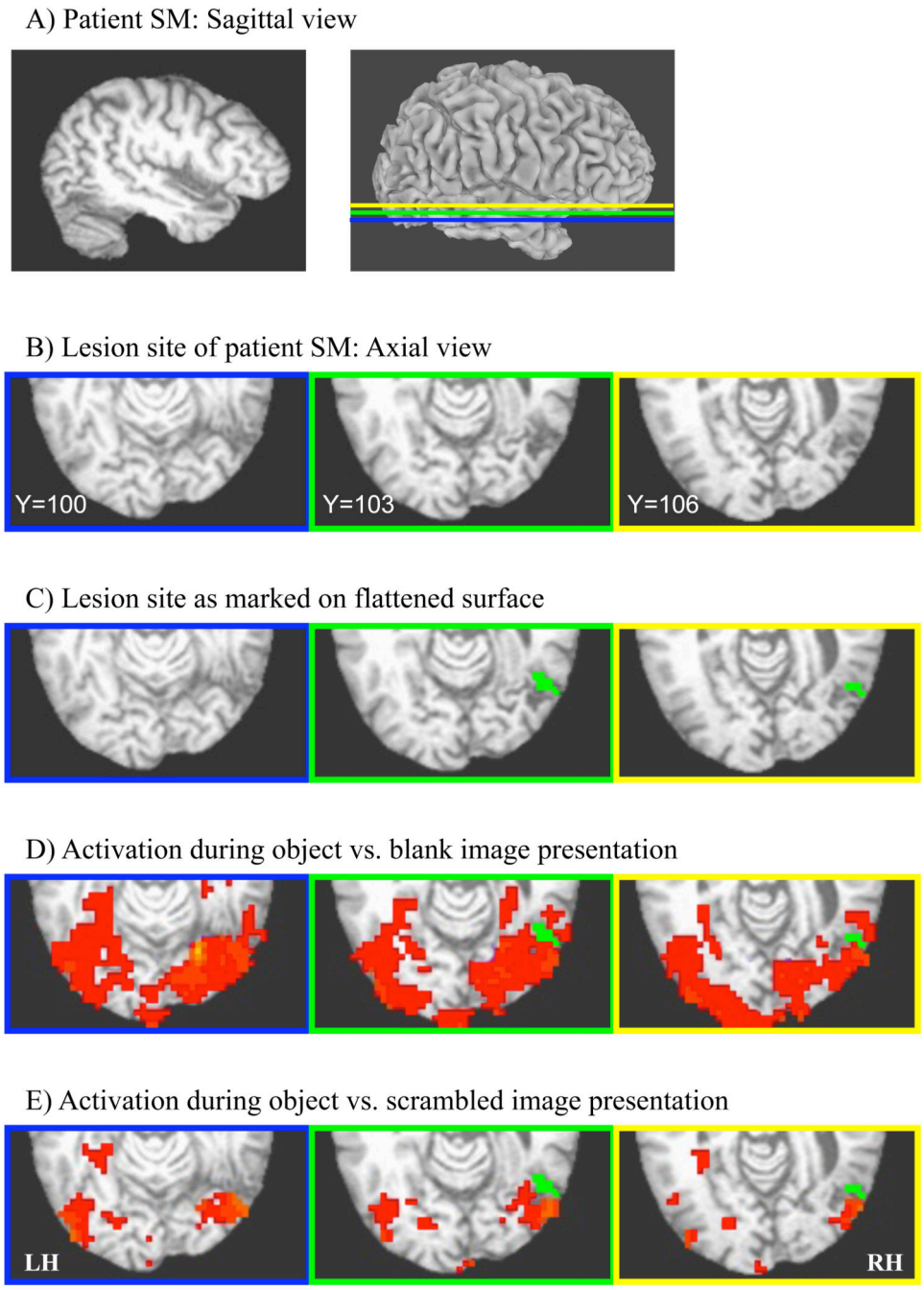

Figure 4. Lesion site of SM in anatomical space. (A) Sagittal view of SM's lesioned hemisphere in anatomical space (left) and inflated (right)

The colors of the overlaid slices correspond to the axial slices shown in B-E. Blue indicates the bottom slice, green indicates the middle slice, and yellow indicates the top slice. Note that the bottom slice is inferior to the lesion, whereas the middle and top slices cover the lesion site. *(B) Axial view of the lesion site.* The slices were cut along the temporal poles for enlarged representation of occipito-temporal cortex. *(C) Axial view of the lesion site (green) as marked on the flattened surface. (D) Activation during object versus blank image*

presentations. (E) Activation during object versus scrambled image presentations. LH=left hemisphere; RH=right hemisphere.

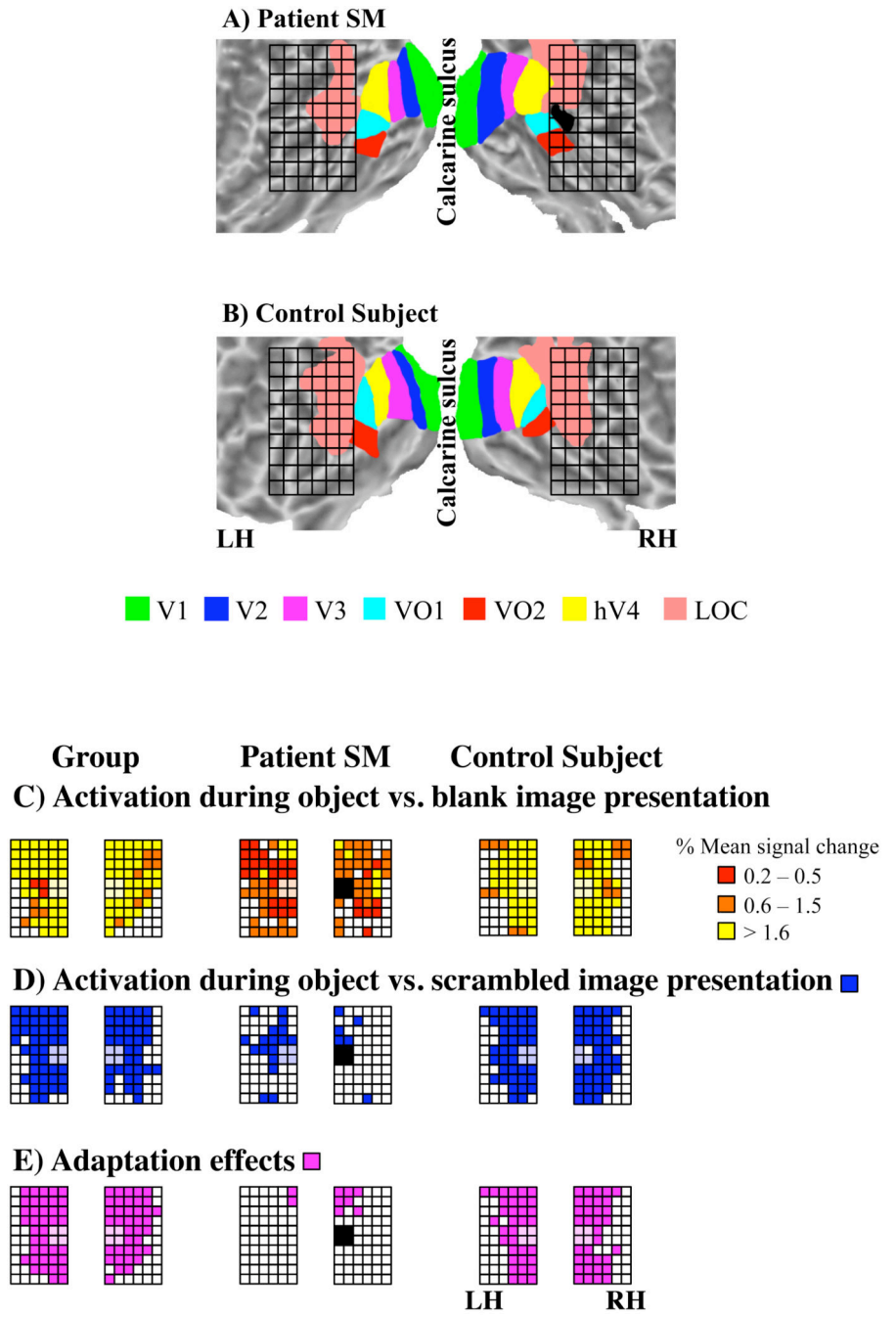

Figure 5. Rectangular grid analysis. (A) Rectangular grid relative to retinotopic cortex in SM

The posterior part of the grid was centered on the lesion site in the RH, and its mirror-symmetric location in the LH. Retinotopic areas and LOC are color-coded. Note that for the functional analysis of grid-sectors, the four sectors encompassing the lesion site, that is, the posterior part of the lateral fusiform gyrus, were excluded. Activations of those sectors are shown black in SM's RH and in transparent colors otherwise. *(B) Rectangular grid relative to retinotopic cortex in control subject C1. (C) Visually-responsive activations in the grid of the group, SM, and control subject C1.* The extent of visually-responsive activations in SM were

similar to the group and C1. The overall magnitude of activations in SM was reduced as compared to the group and C1. *(D) Object-responsive activations in the grid of the group, SM, and C1.* Object-responsive activations in SM were weaker than the group and C1. *(E) Object-selective responses in the grid of the group, SM, and C1.* Object adaptation effects were reduced in SM as compared to the group and C1. LH=left hemisphere; RH=right hemisphere.

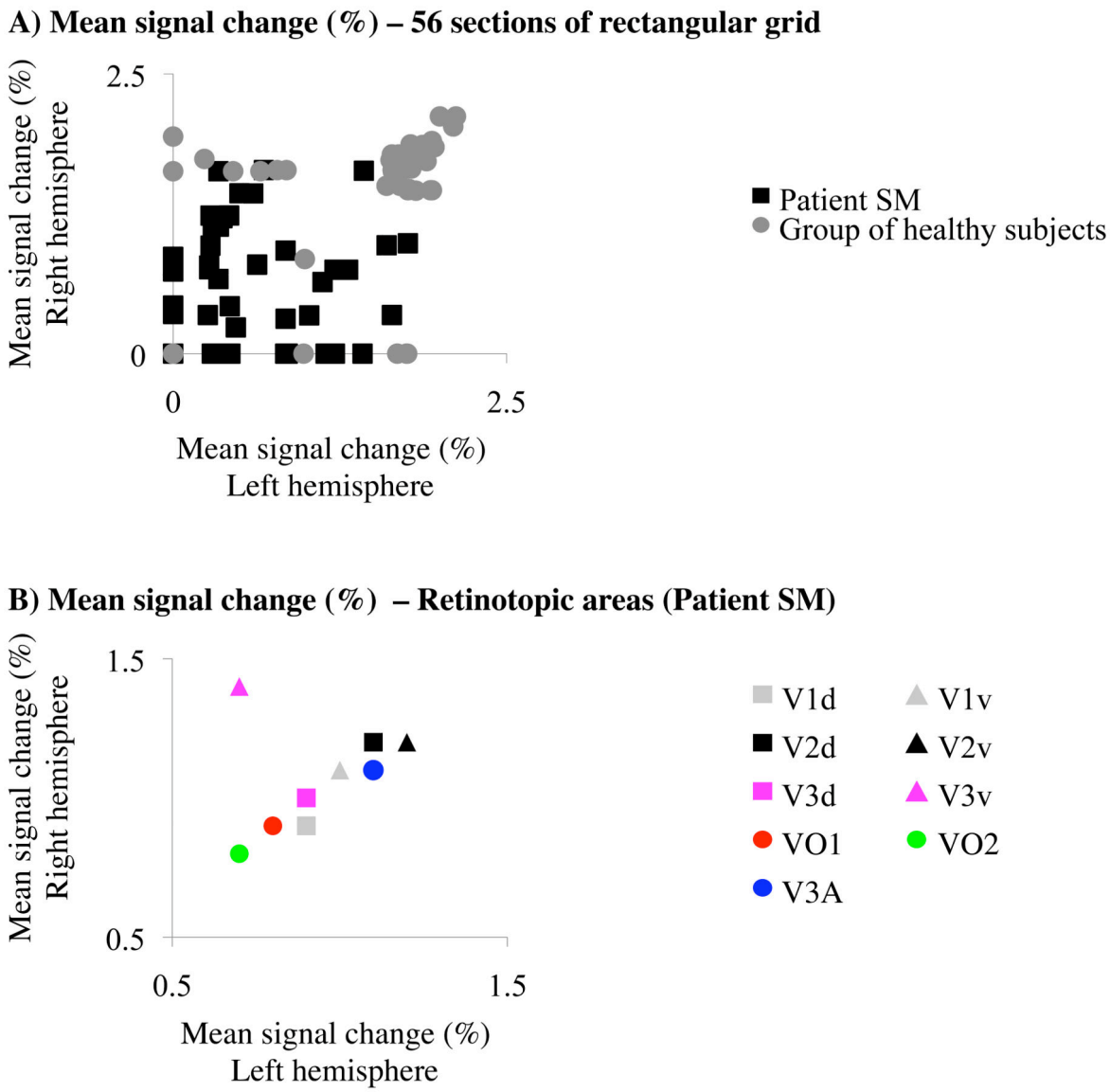

Figure 6. Inter-hemispheric correlations of visually-evoked responses in the group and SM. (A) Mean signal changes in the grid

Unlike the control group, visually-evoked responses were not correlated between the two hemispheres of SM. *(B) Mean signal changes of retinotopic areas.* Similar to control subjects (see Supplementary Fig. 7), visually-evoked responses were correlated between the two hemispheres of SM. Data were volume-corrected (i.e., three voxels within a given grid-sector or 10 voxels within a given retinotopic area were randomly chosen among significantly activated voxels.

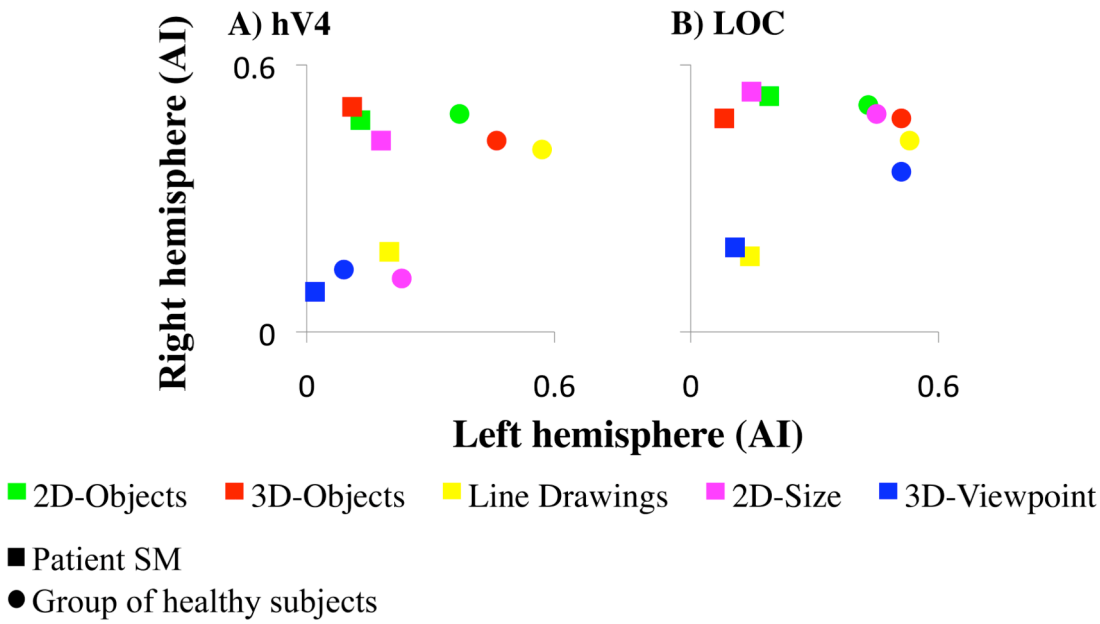

Figure 7. Inter-hemispheric correlations of adaptation effects in hV4 (A) and LOC (B)

The adaptation indices (AIs) for different types of object stimuli are shown for the group (circles) and SM (squares). In contrast to the group, the AIs in hV4 and LOC were not correlated between SM's hemispheres. In the control group, hV4 was size-specific and LOC was viewpoint-invariant. In SM, hV4 was size-invariant and LOC was viewpoint-specific.

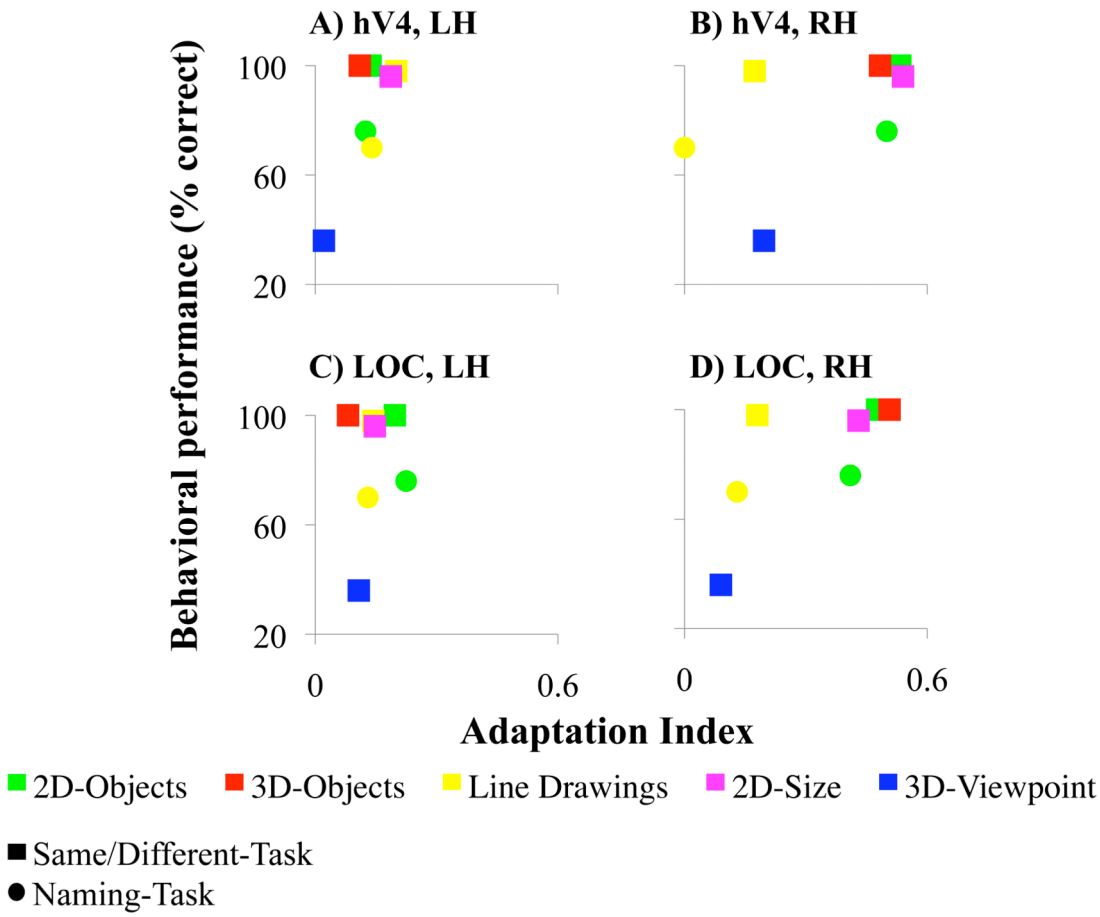

Figure 8. Correlations between SM's behavioral performance and adaptation effects in hV4 (A, B) and LOC (C, D)

Accuracy for the Same/Different-Task (squares) and the Naming-Task (circles) are shown. No obvious relationship was found between SM's behavioral performance and the adaptation indices (AIs) of hV4 and LOC in the LH (A, C). In contrast, a trend towards a systematic relationship was found in both areas of the RH (B, D). Better recognition and higher AIs were observed with 2D- and 3D-objects as well as 2D-objects in different sizes than for line drawings of objects and 3D-objects in different viewpoints. LH=left hemisphere; RH=right hemisphere.